

Effect of Counterion Binding Efficiency on Structure and Dynamics of Wormlike Micelles

C. Oelschlaeger,* P. Suwita, and N. Willenbacher

*Institute for Mechanical Process Engineering and Mechanics, Karlsruhe Institute of Technology (KIT),
76131 Karlsruhe, Germany*

Received November 19, 2009. Revised Manuscript Received February 15, 2010

We have studied the effect of counterion binding efficiency on the linear viscoelastic properties of wormlike micelles formed from hexadecyltrimethylammonium bromide (CTAB) in the presence of different nonpenetrating inorganic salts: potassium bromide (KBr), sodium nitrate (NaNO_3), and sodium chlorate (NaClO_3). We have varied the salt/surfactant ratio R at fixed surfactant concentration of 350 mM. Results are compared to data for the system cetylpyridinium chloride (CPyCl) and the penetrating counterion sodium salicylate (NaSal) (Oelschlaeger, C.; Schopferer, M.; Scheffold, F.; Willenbacher, N. *Langmuir* **2009**, *25*, 716–723). Mechanical high-frequency rheology and diffusing wave spectroscopy (DWS) based tracer microrheology are used to determine the shear moduli G' and G'' in the frequency range from 0.1 Hz up to 1 MHz (Willenbacher, N.; Oelschlaeger, C.; Schopferer, M.; Fischer, P.; Cardinaux, F.; Scheffold, F. *Phys. Rev. Lett.* **2007**, *99*, 068302, 1–4). This enables us to determine the plateau modulus G_0 , which is related to the cross-link density or mesh size of the entanglement network, the bending stiffness κ (also expressed as persistence length $l_p = \kappa/k_B T$) corresponding to the semiflexible nature of the micelles, and the scission energy E_{sciss} , which is related to their contour length. The viscosity maximum shifts to higher R values, and the variation of viscosity with R is less pronounced as the binding strength decreases. The plateau modulus increases with R at low ionic strength and is constant around the viscosity maximum; the increase in G_0 at high R , which is presumably due to branching, is weak compared to the system with penetrating counterion. The scission energy $E_{\text{sciss}} \approx 20 k_B T$ is independent of counterion binding efficiency irrespective of R and is slightly higher compared to the system CPyCl/NaSal, indicating that branching may be significant already at the viscosity maximum in this latter case. The micellar flexibility increases with increasing binding efficiency of counterions according to the Hofmeister series. The persistence length values for systems CTAB/KBr, CTAB/ NaNO_3 , and CTAB/ NaClO_3 are 40, 34, and 29 nm, respectively, independent of R , and are significantly higher than in the case of CPyCl/NaSal.

1. Introduction

Surfactants are amphiphilic molecules composed of two entities: a long hydrophobic tail that has a high affinity with oil and a hydrophilic head that has a high affinity with water. In aqueous solution, such molecules assemble reversibly into a variety of spatially organized structures, whose common feature is the tendency for the hydrophobic tails to avoid contact with water. In the case of charged surfactants, the area per polar head depends strongly on the nature of the counterions and more specifically on their ability to bind to the surfactant molecules. An easy way to induce a morphological variation, for example, spherical micelles to cylindrical micelles, is to decrease the effective headgroup area by adding salt, which screens the electrostatic repulsions between the headgroups and allows them to come closer. So, under appropriate conditions of concentration, salinity, temperature, presence of counterion, etc., surfactants self-assemble into flexible cylindrical micelles, also termed wormlike micelles. If the energy required to break a wormlike micelle into smaller parts, the so-called scission energy, is large enough, the length of the rods can become longer than their persistence length, and they are then similar to semiflexible linear polymer chains. In particular, these flexible wormlike micelles can become entangled, even at fairly low concentration. Wormlike micelles show a strong analogy with conventional polymer chains but have larger diameter ($\sim 1\text{--}10$ nm) and a longer persistence length ($\sim 10\text{--}100$ nm).

Small changes in surfactant structure, the counterion nature¹ and concentration, added electrolytes, or temperature can alter the length, flexibility, and interactions of micelles drastically, resulting in significant effects on macroscopic rheological properties. In particular, various ionic surfactants show a pronounced maximum of the zero-shear viscosity as the salt/surfactant ratio is varied.^{2–7} This is of particular technical interest, since this viscosity maximum is closely related to the application properties of such surfactant systems, but also from a scientific point of view, since the corresponding structural changes are still not really clear. Several studies support the transition from linear to branched micelles; e.g., a combined cryo-TEM, SANS, and rheology study on the system erucylbis(hydroxyethyl)methylammonium chloride (EHAC)/KCl consistently revealed a transition from linear to branched micelles around the viscosity maximum.⁸ In contrast to ordinary polymers these branch points can slide along the micelles and hence provide a high number of degrees of freedom for reptation, resulting in the observed viscosity reduction. In contrast, for the system cetyltrimethylammonium chloride (CTAC) and sodium salicylate (NaSal) cryo-TEM

(2) Candau, S. J.; Khatory, A.; Lequeux, F.; Kern, F. *J. Phys. IV* **1993**, *3*, 197–209.

(3) Khatory, A.; Lequeux, F.; Kern, F.; Candau, S. J. *Langmuir* **1993**, *9*, 1456–1464.

(4) Cappelare, E.; Cressely, R. *Colloid Polym. Sci.* **1998**, *276*, 1050–1056.

(5) Cappelare, E.; Cressely, R. *Rheol. Acta* **2000**, *39*, 346–353.

(6) Raghavan, S. R.; Kaler, E. W. *Langmuir* **2001**, *17*, 300–306.

(7) Schubert, B. A.; Kaler, E. W.; Wagner, N. J. *Langmuir* **2003**, *19*, 4079–4089.

(8) Croce, V.; Cosgrove, T.; Maitland, G.; Hughes, T.; Karlsson, G. *Langmuir* **2003**, *19*, 8536–8541.

*Corresponding author. E-mail: Claude.Oelschlaeger@kit.edu.

(1) Porte, G.; Appell, J. In *Surfactants in Solution*; Mittal, K. L., Lindman, B., Eds.; Plenum: New York, 1984; Vol. 2, p 805.

images did not reveal significant branching around the viscosity maximum, and the viscosity drop was attributed to a change in micellar breakage time.⁹ For systems hexadecyltrimethylammonium bromide (CTAB)^{10,11} and cetylpyridinium chloride (CPyCl) with (NaSal),^{12,13} a strongly binding counterion, even a second viscosity maximum is observed when the salt concentration is further increased. In a recent study¹⁴ Oelschlaeger et al. attribute the first viscosity maximum to a transition from linear to branched micelles, the second viscosity increase to a decrease of the branching density accompanied by an increase of micelle length, and the second viscosity decrease to a shortening of the micelles with an increase of the branching density.

In the present study we use a recently established experimental approach¹⁵ combining mechanical high-frequency rheology and optical microrheology to determine the linear viscoelastic properties of surfactant solutions in the frequency range from 0.1 Hz up to 1 MHz. This provides new insight into structural and dynamic changes accompanying the characteristic viscosity maximum observed in systems formed by the cationic surfactant hexadecyltrimethylammonium bromide (CTAB) in presence of different inorganic salts: potassium bromide (KBr), sodium nitrate (NaNO₃), and sodium chlorate (NaClO₃). These counterions are nonpenetrating counterions, and they differ by their polarizability effect, i.e., their binding efficiency. This efficiency increases according to the sequence

$$F^- < Cl^- < Br^- < NO_3^- < ClO_3^-$$

The above sequence is what is expected from the Hofmeister series. Most of the previous studies related to the Hofmeister effect on micellar solutions deal with its impact on the micellization (cmc) process.^{16–20} The trend for micellization basically follows the Hofmeister series. Recently, Danino et al.²¹ investigated the counterion effect on the transition from spherical to cylindrical micelles and on micellar growth. They showed that the transition from spherical to rodlike or wormlike micelles occurs at lower salt concentrations, and longer micelles are formed as the binding efficiency increases. Moreover, the penetrating counterion (NaSal) induces even stronger structural changes compared to the nonpenetrating salts. For each system we investigate the variation of the plateau modulus G_0 , the scission energy E_{sciss} , and the persistence length l_p with salt/surfactant ratio R at constant surfactant concentration of 350 mM CTAB. Despite the large amount of literature for these systems, no results on the scission energy and bending stiffness are available so far. The results obtained here are systematically compared with those

obtained in ref 14 for a system formed by the cationic surfactant (CPyCl) and a penetrating counterion (NaSal).

2. Structure and Dynamics of WLM

The growth of cylindrical micelles is controlled by the competition between the entropy of mixing and the scission energy E_{sciss} . For neutral micelles, the scission energy is equal to the end-cap energy that is the energy required to create two end-caps from a semi-infinite cylinder. The length distribution in electrostatically screened solutions of wormlike micelles undergoing reversible scission can be obtained from the models derived for “conventional” polymers but taking into account the two specific features of equilibrium polymer solutions: (i) the average length of the micelles is determined by the thermodynamical equilibrium of the solution; (ii) the micelles continuously break and recombine. The overall length of the micelles is referred to as the contour length L and varies between a few nanometers to micrometers. A mean field treatment of the growth process for highly screened micelles has been obtained from the models derived by Cates^{22,23} and predicts an exponential distribution of length $N(L)$ ²⁴

$$N(L) \propto \exp\left(-\frac{L}{\bar{L}}\right) \quad (1)$$

with the average length given by

$$\bar{L} \cong \varphi^{0.5} \exp\left(\frac{E_{\text{sciss}}}{2k_B T}\right) \quad (2)$$

where φ is the surfactant volume fraction and T the temperature. Slight changes in the composition of surfactant solutions affect their overall length, which is directly related to the scission energy. For charged systems this quantity has two contributions:

$$E_{\text{sciss}} = E_c - E_e \quad (3)$$

E_c is the energy required to create two hemispherical end-caps as a result of scission of the wormlike micelles and reflects the differences in surfactant packing in the end-caps vs the cylindrical body of the micelles. For nonionic micelles or for ionic micelles at high ionic strength $E_{\text{sciss}} = E_c$. For ionic micelles repulsion between charged head groups favors micelle breaking and lowers E_{sciss} , this effect is summarized in E_e . The scission energy E_{sciss} is related to the temperature dependence of the moduli G' and G'' at intermediate frequencies, in the so-called entanglement regime, where G' exhibits a plateau and G'' ($\ll G'$) goes through a minimum. In this regime the ratio G''_{min}/G_0 is related to l_e (contour length between two successive entanglements), \bar{L} , and E_{sciss} according to²⁵

$$\frac{G''_{\text{min}}}{G_0} \sim \frac{l_e}{\bar{L}} \sim \varphi^{-1.85} \exp\left(-\frac{E_{\text{sciss}}}{2k_B T}\right) \quad (4)$$

In the case of formation of branched micelles which correspond to the formation of equilibrium cross-links arising through local fusion of micelles, a model based on the coupled reptation/reaction for branched micelles was developed by Lequeux.²⁶ In the frame of this model, all the results concerning the rheology of

(9) Clausen, T.; Vinson, P. K.; Minter, J. R.; Davis, H. T.; Talmon, Y.; Miller, W. G. *J. Phys. Chem.* **1992**, *96*, 474–484.

(10) Nemoto, N.; Kuwahara, M.; Yao, M.-L.; Osaki, K. *Langmuir* **1995**, *11*, 30–36.

(11) Galvan-Miyoshi, J.; Delgado, J.; Castillo, R. *Euro. Phys. J. E* **2008**, *26*, 369–377.

(12) Rehage, H.; Hoffmann, H. *J. Phys. Chem.* **1988**, *92*, 4712–4719.

(13) Rehage, H.; Hoffmann, H. *Mol. Phys.* **1991**, *74*, 933–973.

(14) Oelschlaeger, C.; Schopferer, M.; Scheffold, F.; Willenbacher, N. *Langmuir* **2009**, *25*, 716–723.

(15) Willenbacher, N.; Oelschlaeger, C.; Schopferer, M.; Fischer, P.; Cardinaux, F.; Scheffold, F. *Phys. Rev. Lett.* **2007**, *99*, 068302, 1–4.

(16) Maiti, K.; Mitra, D.; Guha, S.; Moulik, S. P. *J. Mol. Liq.* **2009**, *146*, 44–51.

(17) Vlachy, N.; Jagoda-Cwiklik, B.; Vacha, R.; Touraud, D.; Jungwirth, P.; Kunz, W. *Adv. Colloid Interface Sci.* **2009**, *146*, 42–47.

(18) Jiang, N.; Li, P.; Wang, Y.; Wang, J.; Yan, H.; Thomas, R. K. *J. Phys. Chem. B* **2004**, *108*, 15385–15391.

(19) Jiang, N.; Li, P.; Wang, Y.; Wang, J.; Yan, H.; Thomas, R. K. *J. Colloid Interface Sci.* **2005**, *286*, 755–760.

(20) Boström, M.; Williams, D. R. M.; Ninham, B. W. *Langmuir* **2002**, *18*, 6010–6014.

(21) Abezgauz, L.; Kuperkar, K.; Hassan, P. A.; Ramon, O.; Bahadur, P.; Danino, D. *J. Colloid Interface Sci.* **2010**, *342*, 83–92.

(22) Cates, M. E. *J. Phys. (Paris)* **1988**, *49*, 1593–1600.

(23) Cates, M. E. *Macromolecules* **1987**, *20*, 2289–2296.

(24) Israelachvili, J.; Mitchell, D. J.; Ninham, B. W. *J. Chem. Soc., Faraday Trans. 2* **1976**, *72*, 1525–1568.

(25) Granek, R.; Cates, M. E. *J. Chem. Phys.* **1992**, *96*, 4758–4767.

(26) Lequeux, F. *Europhys. Lett.* **1992**, *19*, 675–681.

linear wormlike micelles can be applied to branched micelles, provided that one substitutes \bar{L} by \bar{L}_c , where \bar{L}_c represents the harmonic mean between the average distance from one point along the micelle to the first cross-link and the average distance from that point to the first end-cap. Consequently, we determine the scission energy using the same method (section 4.2.3) for linear as well as for branched micelles. Another key structural parameter for wormlike micellar solutions investigated here is the plateau modulus G_0 . This parameter, determined at intermediate frequencies, is directly related to the mesh size ξ of the system with $G_0 \sim \xi^{-3}$ and is typically independent of temperature.¹⁵ We also investigate the shear moduli in the high-frequency range; the stress relaxation is controlled by the internal dynamics of individual micelles, and the moduli G' and G'' show characteristic scaling behavior:

$$G' \sim G'' \sim \omega^\alpha \quad (5)$$

First the Rouse–Zimm modes dominate and $\alpha = 1/2$ – $2/3$. At even higher frequencies internal bending modes of single Kuhn segments determine G' and G'' , and hence these dynamic parameters are related to the bending modulus κ as a structural parameter; κ is often expressed in terms of the persistence length $\kappa = k_B T l_p$. In this frequency range, the scaling exponent $\alpha = 3/4$ as predicted by Morse²⁷ and Gittes and McKintosh.²⁸ Accordingly, the persistence length l_p can be determined from the absolute values of G' and G'' in the $\alpha = 3/4$ scaling regime from a relationship based on a statistical mechanical treatment of the single filament stress response of semiflexible chains²⁸

$$G^* = \frac{\rho}{15} \kappa l_p \left(\frac{-2i\zeta}{\kappa} \right)^{3/4} \omega^{3/4} - i\omega\eta_s \quad (6)$$

where ζ is the lateral drag coefficient and ρ the area density of micelles. The latter can be calculated as $\rho = \phi_{\text{surf}} / ((\pi/4)d_{\text{mic}}^2)$, where ϕ_{surf} is the surfactant concentration (v/v) and $(\pi/4)d_{\text{mic}}^2$ is the cross-sectional area of the micelles. Recently, we have demonstrated that the high frequency range where the $\omega^{3/4}$ scaling occurs can be accessed by optical as well as mechanical rheometry. Both techniques can be used to determine l_p according to eq 6, and l_p values down to a few nanometers are accessible.¹⁵ All these structural features, the characteristic length scales, and the corresponding characteristic relaxation times strongly depend not only on the chemical nature and concentration of the surfactant or surfactant mixture under consideration but also on the nature and concentration of the counterion (binding vs non-binding) and the ionic strength of the solution. This has been studied intensively not only by rheological experiments but also using electron microscopy and various scattering techniques.^{7,29–31} Cryo-TEM, for example, has been used to visualize entanglements, branching, and the semiflexible, wormlike nature of the micelles directly.^{8,9,32–34}

In the first part of this paper we compare rheological results from mechanical rheometry and optical microrheology for systems with nonpenetrating salt, namely, CTAB/KBr, CTAB/

NaNO₃, and CTAB/NaClO₃. We focus on three different parameters: zero-shear viscosity, plateau modulus, and scission energy. In the second part of the paper, we investigate the effect of salt concentration on these parameters but also on the persistence length and compare the results with a system formed from the cationic surfactant (CPyCl) and the penetrating salt (NaSal).

3. Materials and Methods

3.1. Sample Characteristics. Products used in this work are commercially available; they were purchased from Carl Roth GmbH (Karlsruhe, Germany). Aqueous solutions of surfactant/counterion mixtures hexadecyltrimethylammonium bromide/potassium bromide (CTAB/KBr), sodium nitrate (CTAB/NaNO₃), and sodium chlorate (CTAB/NaClO₃) were investigated here. The CTAB concentration has been kept constant at 350 mM. At this concentration the three systems exhibit pronounced viscoelastic behavior over a broad salt concentration and temperature range. For the CPyCl/NaSal system, the CPyCl concentration was 100 mM.¹⁴ The sample solutions were prepared by gently stirring the surfactant and salt in deionized water. For equilibrium measurements, they were stored for at least 1 day at the desired temperature: 35 °C for the CTAB/KBr system, 30 °C for the CTAB/NaNO₃ and CTAB/NaClO₃ systems, and 20 °C for the CPyCl/NaSal system.

3.2. DWS-Based Optical Microrheology. DWS uses the equilibrium thermal response of small (colloidal) particles embedded in a material to obtain quantitative information about the macroscopic loss and storage moduli, $G'(\omega)$ and $G''(\omega)$, over an extended range of frequencies. This is based on a quantitative relationship between the tracer mean-squared displacement $\langle \Delta r^2(t) \rangle$ and the complex shear modulus $G^*(\omega) = G'(\omega) + iG''(\omega)$.³⁵ The Laplace transform of the particle mean-squared displacement $\langle \Delta r^2(i\omega) \rangle$ is related to the complex modulus of the sample via a generalized Stokes–Einstein equation (GSE):

$$G^*(\omega) = \frac{k_B T}{\pi a \omega \langle \Delta r^2(i\omega) \rangle} = G'(\omega) + iG''(\omega) \quad (7)$$

For a quantitative interpretation of the raw experimental data $\langle \Delta r^2(t) \rangle$, the Laplace transformation, is the most critical part of the analysis. To reduce truncation errors, we apply a procedure suggested by Mason et al.,³⁶ and $\tilde{G}(s)$ is estimated by substituting $\langle \Delta r^2(t) \rangle$ into an algebraic Stokes–Einstein form:³⁷

$$\tilde{G}(s) = \frac{k_B T}{\pi a \langle \Delta r^2(t) \rangle \Gamma[1 + (\partial \ln \langle \Delta r^2(t) \rangle / \partial t)]} \Big|_{t=1/s} \quad (8)$$

In order to reduce scatter, we first fit $\langle \Delta r^2(t) \rangle$ with a polynomial of order 6 or 7 and then use eq 8 to extract the moduli $G'(\omega)$ and $G''(\omega)$. The choice of the polynomial order and the range of data selected do not influence the results significantly.¹⁵ Finally, it is worthwhile to note that, contrary to mechanical measurements, the in- and out-of-phase contributions are not measured independently but have to be extracted from a single value of the slope $\partial \ln \langle \Delta r^2(t) \rangle / \partial t$. As a consequence, if $G'(\omega)$ and $G''(\omega)$ are of different magnitude, the lower value extracted from DWS measurements is often not very well-defined. At times shorter than 10^{-5} s, or frequencies above $\omega = 10^5$ rad/s, inertia effects become significant,³⁸ and a simple, self-consistent correction scheme is used to account for that.¹⁵ The influence of fluid inertia is determined by

(27) Morse, D. C. *Phys. Rev. E* **1998**, *58*, R1237–R1240.

(28) Gittes, F.; MacKintosh, F. C. *Phys. Rev. E* **1998**, *58*, R1241–R1244.

(29) Shikata, T.; Dahman, S. J.; Pearson, D. S. *Langmuir* **1994**, *10*, 3470–3476.

(30) Cates, M. E.; Candau, S. J. *J. Phys.: Condens. Matter* **1990**, *2*, 6869–6892.

(31) Magid, L. J.; Li, Z.; Butler, P. D. *Langmuir* **2000**, *16*, 10028–10036.

(32) Lin, Z. *Langmuir* **1996**, *12*, 1729–1737.

(33) Bernheim-Groswasser, A.; Wachtel, E.; Talmon, Y. *Langmuir* **2000**, *16*, 4131–4140.

(34) Bernheim-Groswasser, A.; Zana, R.; Talmon, Y. *J. Phys. Chem. B* **2000**, *104*, 12192–12201.

(35) Mason, T. G.; Weitz, D. A. *Phys. Rev. Lett.* **1995**, *74*, 1250–1253.

(36) Mason, T. G.; Ganesan, K.; van Zanten, J. H.; Wirtz, D.; Kuo, S. C. *Phys. Rev. Lett.* **1997**, *79*, 3282–3285.

(37) von Berlepsch, H.; Harnau, L.; Reineker, P. *J. Phys. Chem. B* **1998**, *102*, 7518–7522.

(38) Weitz, D. A.; Pine, D. J.; Pusey, P. N.; Though, R. J. A. *Phys. Rev. Lett.* **1989**, *63*, 1747–1750.

the high-frequency viscosity.³⁹ Here we have estimated an effective high-frequency viscosity of ~ 3 mPa s in the regime $\omega = 10^5$ – 10^6 s⁻¹ by extrapolating the $\omega < 10^5$ s⁻¹ data for $G''(\omega)$ from mechanical measurements. We then correct the particle mean-square displacement for inertia effects based on the theory of Hinch⁴⁰ developed for the motion of a sphere in a simple fluid with viscosity η . In a second iteration step we again fit the resulting loss modulus and repeat this procedure several times. In our case the correction factor attains its smallest value of 0.7 for the shortest time analyzed $\tau = 5 \times 10^{-7}$ s. More details about the DWS device and data processing used here can be found in ref 14.

3.3. Squeeze Flow. Oscillatory squeeze flow experiments were performed using a piezo-driven axial vibrator (PAV) customized at the Institute for Dynamic Material Testing (Ulm, Germany). The general theory of squeeze flow is covered in standard textbooks of fluid mechanics.⁴¹ The theory of the PAV as well as the mechanical and electronic setup used here are thoroughly discussed elsewhere,^{14,42,43} and therefore this is summarized here only briefly. In our squeeze flow experiments the samples are placed into a gap between two stainless steel plates. The lower plate is supported by a thin-walled quadratic copper tube carrying the piezo-elements, which exert the vibrational motion and pick up the response signal. This lower part of the device is surrounded by a double-walled cylinder allowing for circulation of a thermostating fluid, and the sample temperature is controlled with an accuracy of ± 0.1 °C. The upper boundary of the gap is a thick metal lid, which provides complete sealing of the fluid. The instrument operates at constant force amplitude, and from the ratio of the dynamic displacement of the lower plate (amplitude ~ 5 nm) with and without fluid the complex squeeze stiffness K^* of the fluid is obtained which is directly related to the complex shear modulus G^* :⁴³

$$K^* = \frac{3\pi R^4}{2d^3} G^* \left(1 + \frac{\rho\omega^2 d^2}{10G^*} + \dots \right) \quad (9)$$

where ρ is the fluid density, R (here 10 mm) is the radius, and d is the height of the gap. The denominator in eq 9 is a series expansion taking into account the inertia of the fluid in the gap. The determination of G^* strongly depends on the exact knowledge of d , which is determined by calibration using Newtonian liquids with viscosities between 1 and 2000 mPa s. Gap heights between 39 and 50 μ m have been used here, corresponding to sample volumes between 100 and 200 μ L. Moduli G' or G'' in the range from 0.1 Pa to 10 kPa are accessible with the setup described here.

3.4. Rotational Rheometry. A rotational rheometer Thermo MARS II equipped with a cone-plate measuring cell (diameter $d_{CP} = 35$ mm, cone angle $\alpha_{cone} = 4^\circ$) was used to perform as well as static and small-amplitude oscillatory shear experiments covering the frequency range from 0.01 to 100 rad s⁻¹ at a strain amplitude $\gamma_0 = 0.1$. Strain sweep experiments performed prior to the frequency sweeps confirm that this strain amplitude is sufficiently small to provide a linear material response at all investigated frequencies. A solvent trap was used to avoid evaporation of the sample during the experiment.

4. Results and Discussion

4.1. Comparison of Mechanical Rheometry and DWS Measurements.

The variation of the dynamic shear moduli G'

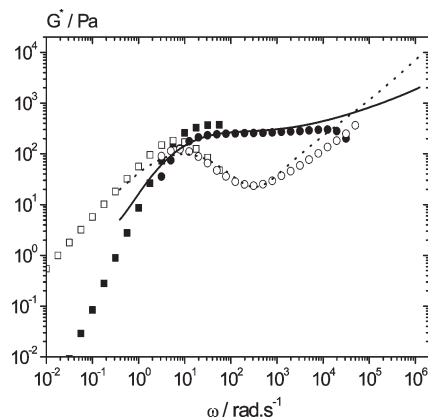


Figure 1. Dynamic shear moduli G' and G'' of an aqueous solution of 350 mM CTAB/600 mM NaClO₃ obtained from DWS (G' , solid line; G'' , dotted line), oscillatory squeeze flow (G' , closed circles; G'' , open circles) and rotational rheometry (G' , closed squares; G'' , open squares).

and G'' as a function of frequency as determined from mechanical and optical rheometry is given in Figure 1 for the system CTAB/NaClO₃ at $R = 1.71$. Similar results were obtained for all systems investigated here, in particular a well-developed plateau in G' , which extends at least over 2 decades in frequency, is observed even at the highest salt/surfactant ratios. Generally, good agreement is found between mechanical and optical methods. For both techniques, the shapes of the relaxation spectra coincide very well over the whole frequency range, and since also the absolute values agree very well, curves have not been shifted to match the data. Similar results have been obtained for the two other systems: CTAB/KBr and CTAB/NaNO₃. Nevertheless, in some experiment we observe a slight difference in the variation of the moduli just after the minimum of G'' . In particular, G'' from DWS measurements increases more rapidly than G'' from squeeze flow measurements. This difference may be attributed to uncertainties in the DWS calculation process. Indeed, in an oscillatory shear experiment the real and imaginary parts of $G^*(\omega)$ are determined from the amplitude and phase shift of the response signal. Such a phase analysis is much more accurate than the DWS data treatment, where the mean-squared displacement is measured in time space. The characteristic rheological parameters—terminal relaxation time T_R (Figure 2a) and plateau modulus G_0 (Figure 2b)—have been extracted from both mechanical and optical rheological techniques as a function of salt/surfactant ratio R for the systems CTAB/KBr (A), CTAB/NaNO₃ (B), and CTAB/NaClO₃ (C). T_R and G_0 are directly deduced from the modulus curves. T_R is given by the inverse angular frequency corresponding to the first crossover between G' and G'' . For DWS and oscillatory squeeze flow, G_0 is determined as the value of the modulus G' at the frequency at which G'' has its local minimum, G''_{min} . For rotational rheometry G_0 is taken as the value of G' where it exhibits a constant plateau, since the minimum in G'' is not accessible with this technique. We observe for all the systems and at all salt concentrations good agreement in the determination of G_0 between the different techniques. This is different compared to the micellar systems formed with penetrating counterion: CTAB/NaSal and CPyCl/NaSal, investigated by Galvan-Miyoshi et al.¹¹ and Oelschlaeger et al.,¹⁴ respectively. In those studies strong deviations (up to factor 4.5) between G_0 values deduced from DWS and those from mechanical techniques were found especially at high salt concentrations most likely due to aggregation of tracer particles. The agreement between T_R data

(39) Ladd, A. J. C.; Gang, H.; Zhu, J. X.; Weitz, D. A. *Phys. Rev. Lett.* **1995**, *74*, 318–321.

(40) Hinch, E. J. *Fluid Mech.* **1975**, *72*, 499–511.

(41) Bird, R. B.; Armstrong, R. C.; Hassager, O. Dynamics of Polymeric Liquids. In *Fluid Dynamics*, 2nd ed.; Wiley: New York, 1987; Vol. 1, p 784.

(42) Crassous, J. J.; Regisser, R.; Ballauff, M.; Willenbacher, N. *J. Rheol.* **2005**, *49*, 851–863.

(43) Kirschenmann, L. Ph.D. Thesis, Institut für Dynamische Materialprüfung, University of Ulm, **2003**.

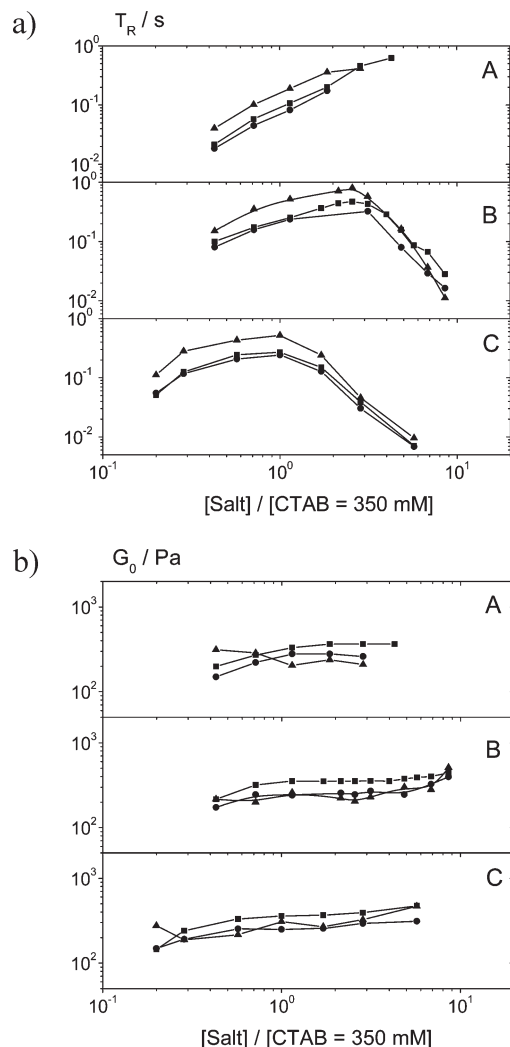


Figure 2. Terminal relaxation time T_R (a) and plateau modulus G_0 (b) as a function of $[\text{salt}]/[\text{CTAB}]$ at constant surfactant concentration of 350 mM CTAB obtained from DWS (triangles), oscillatory squeeze flow (circles), and rotational rheometer (squares): (A) CTAB/KBr, (B) CTAB/NaNO₃, and (C) CTAB/NaClO₃. All error bars are as large as the size of the different symbols.

from different mechanical methods is also very good, but irrespective of the nature of the salt T_R values from DWS are up to a factor of 2 higher than the corresponding mechanical data. This is most likely due to the limitations of our DWS setup with respect to long measurement times, when the signal-to-noise ratio is low.

4.2. Effect of Salt on Structural and Dynamic Properties.

All results concerning the CPyCl/NaSal system are reproduced from Oelschlaeger et al.¹⁴ Only a new l_p calculation has been performed after correction of the loss moduli for the solvent (water) contribution in oscillatory squeeze flow measurements.

4.2.1. Zero-Shear Viscosity. The variation of the zero-shear viscosity η_0 versus added salt at fixed surfactant concentration for systems CTAB/NaClO₃, CTAB/NaNO₃, CTAB/KBr, and CPyCl/NaSal is given in Figure 3. The first observation is that, in contrast to the system CPyCl with the penetrating counterion NaSal, the CTAB solutions with nonpenetrating counterions (NaClO₃ and NaNO₃) exhibit only one viscosity maximum. No maximum occurs for the system with added KBr in the salt concentration range investigated here, and with higher KBr

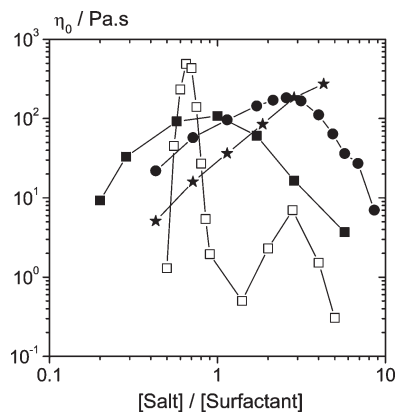


Figure 3. Variation of the zero-shear viscosity η_0 as a function of $R = [\text{salt}]/[\text{surfactant}]$ at constant surfactant concentration of 350 mM CTAB and 100 mM CPyCl obtained from rotational rheometer measurements: CPyCl/NaSal (open squares, data redrawn from ref 14), CTAB/NaClO₃ (solid squares), CTAB/NaNO₃ (solid circles), and CTAB/KBr (solid stars).

concentration the salt does not dissolve anymore in water. These findings are in agreement with literature data for other surfactant concentration.^{2–4,44,45} The second observation is that more salt is needed to reach the viscosity maximum for the systems with nonpenetrating salt compared to the system with penetrating salt. The viscosity maximum occurs earlier with increasing affinity of the counterion to the surfactant; η_0 occurs at $R = 0.65$, $R = 1$, and $R = 2.5$ for systems CPyCl/NaSal (first maximum), CTAB/NaClO₃, and CTAB/NaNO₃, respectively. Also, the viscosity peak for the system with penetrating salt reaches ~ 1000 Pa s, compared to a zero-shear viscosity value of ~ 100 Pa s observed for nonpenetrating salts. Finally, the change of viscosity with salt/surfactant ratio (slope of the $\eta_0(R)$ curve) is much higher for penetrating salt compared with that for nonpenetrating salt. All these results indicate that the addition of penetrating salt has much stronger effect on the micellar structure and properties than the addition of nonpenetrating salt.

4.2.2. Plateau Modulus. Almost all of the literature dealing with the linear viscoelastic properties of wormlike micelles is based on data from small-amplitude oscillatory shear experiments performed by conventional rotational rheometry and are thus limited to the frequency range $\omega < 100$ rad/s. In order to provide the most accurate data at intermediate frequencies between 10 and 10^4 rad/s, we used oscillatory squeeze flow measurements to determine the plateau modulus G_0 , which is related to the crosslink density or mesh size ξ of the entanglement network. Corresponding values for ξ are summarized in Table 1. Figure 4a–d shows the variation of the plateau modulus as a function of ionic strength for the different systems investigated. A common observation is a strong and rapid increase in the plateau modulus at very low salt content corresponding to a strong increase of the zero-shear viscosity (solid line). This first G_0 increase is due to the formation and increase in the number of entanglements accompanying the growth of the linear micelles. Since such wormlike micelles exhibit a broad distribution of chain length, more and more micelles contribute to the entanglement network as the average length increases. This interpretation is further confirmed by the temperature dependence of the plateau modulus. For all systems investigated in this study and at all salt concentrations, G_0 was measured at four different temperatures (35, 40, 45, and

(44) Kuperkar, K.; Abezgauz, L.; Danino, D.; Verma, G. *J. Colloid Interface Sci.* **2008**, *323*, 403–409.

(45) Kuperkar, K.; Abezgauz, L.; Danino, D.; Verma, G.; Hassan, P. K.; Aswal, P. K.; Varade, D.; Bahadur, P. *PRAMANA J. Phys.* **2008**, *71*, 1003–1008.

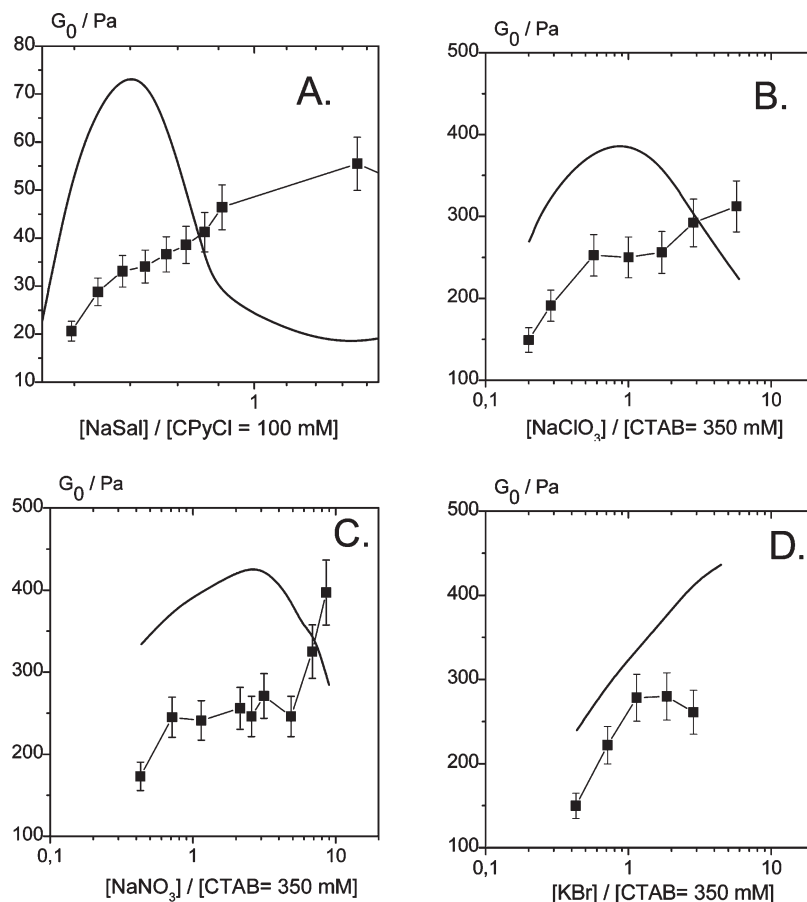


Figure 4. Variation of the plateau modulus G_0 as a function of $R = [\text{salt}]/[\text{surfactant}]$ at constant surfactant concentration of 350 mM CTAB and 100 mM CPyCl obtained from oscillatory squeeze flow measurements: (A) CPyCl/NaSal (data redrawn from ref 14), (B) CTAB/NaClO₃, (C) CTAB/NaNO₃, and (D) CTAB/KBr. The solid line represents the variation of the zero-shear viscosity η_0 in arbitrary units.

Table 1. Rheological Parameters: Effect of Salt Concentration

R	ξ (nm)	G''_{\min} (Pa)	l_e (nm)	L (nm)	l_p (nm)	κ^{-1} (nm)	$l_{p,e}$ (nm)
CTAB/NaClO ₃							
0.2	30.3	50.8	30.3	88.9	34.2	1.15	0.460
0.286	27.9	30.7	26.5	164.8	27.1	0.96	0.320
0.571	25.5	19.8	22.8	290.6	28.0	0.68	0.160
1	25.5	17.6	22.9	325.0	25.4	0.51	0.090
1.714	25.3	24.0	22.6	240.0	29.8	0.39	0.054
2.857	24.2	42.0	21.0	146.0	30.8	0.30	0.032
5.714	23.7	71.7	20.3	88.3	29.5	0.21	0.016
CTAB/NaNO ₃							
0.429	28.9	32.2	26.1	140	33.6	0.78	0.210
0.714	25.7	24.9	23.0	226	30.4	0.60	0.130
1.143	25.9	19.8	22.6	274	31.7	0.48	0.080
2.143	25.3	18.8	20.9	284	33.8	0.35	0.040
2.571	25.7	16.7	20.6	303	35.7	0.32	0.035
3.143	24.9	21.0	19.8	255	35.1	0.29	0.030
4.857	25.7	24.8	20.3	204	36.4	0.23	0.020
6.857	23.4	37.8	18.9	162	32.2	0.19	0.013
8.571	21.9	52	15.6	120	36.4	0.17	0.010
CTAB/KBr							
0.429	30.5	55.4	25.3	68	39.4	0.78	0.22
0.714	26.7	39.2	20.4	115	39.2	0.61	0.13
1.143	24.8	34.0	18.0	147	41.5	0.48	0.08
1.857	24.8	24.8	17.9	202	40.2	0.38	0.05
2.857	25.3	17.9	18.7	272		0.30	0.03

50 °C). G_0 is independent of temperature at intermediate and high salt/surfactant ratios, although the micellar length decreases with

increasing temperature, as indicated by the shift of the terminal flow regime to higher frequencies. But at the lowest salt concentrations a slight decrease of the modulus with temperature is found. This again indicates that the fraction of micelles contribution to the entanglement network decreases with increasing temperature as the micellar length decreases.

At higher salt content and for the system with penetrating salt (Figure 4a), G_0 continues to increase with ionic strength, increasing by a factor of 2 from $R = 0.7$ to 1.4; this corresponds to the region between the maximum and minimum of η_0 . Cryo-TEM pictures taken for the same salt/surfactant system, but at a surfactant concentration of 15 mM, clearly show a transition from linear to branched micelles at the first maximum of η_0 , with the branching density increasing as the minimum of η_0 ^{21,46} is approached. Thus, this second G_0 increase can be attributed to an additional contribution of branching points to the cross-link density. For systems with nonpenetrating salt, CTAB/NaClO₃ (Figure 4b) and CTAB/NaNO₃ (Figure 4c), G_0 is independent of salt concentration around the viscosity maximum but increases by a factor of 1.2 and 1.6, respectively, at very high salt content. For these two systems we can hypothesize, as for the CPyCl/NaSal system, that this slight increase of G_0 can be attributed to the formation of branched micelles, but by a less significant number compared to the CPyCl/NaSal system. Cryo-TEM images of the CTAB/NaNO₃ system⁴⁴ showing a small number of micellar

(46) Abezgauz, L.; Ramon, O.; Danino, D. Department of Biotechnology and Food Engineering, Technion, Haifa, Israel. European Colloid and Interface Society, Geneva, 2007.

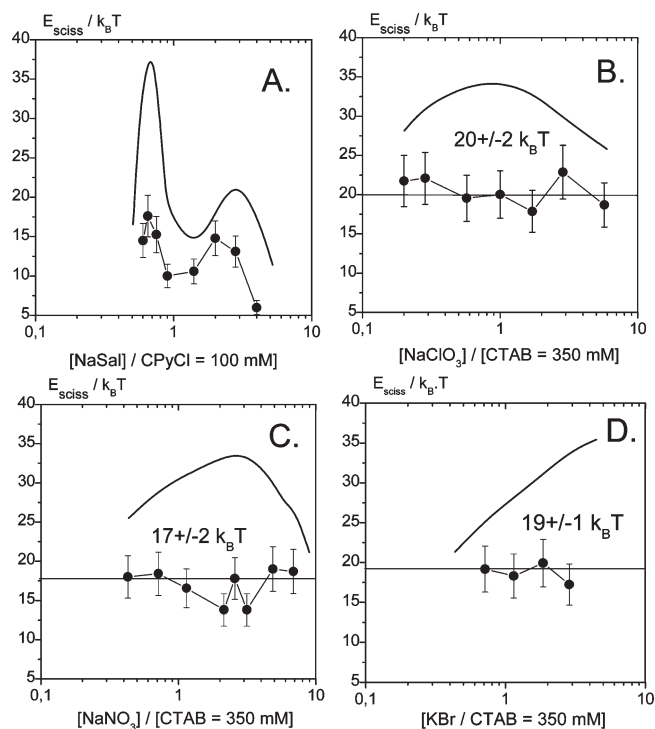


Figure 5. Variation of the scission energy E_{sciss} as a function of $R = [\text{salt}]/[\text{surfactant}]$ at constant surfactant concentration of 350 mM CTAB and 100 mM CPyCl obtained from oscillatory squeeze flow measurements: (A) CPyCl/NaSal (data redrawn from ref 14), (B) CTAB/NaClO₃, (C) CTAB/NaNO₃, and (D) CTAB/KBr. The solid line represents the variation of the zero-shear viscosity η_0 in arbitrary units.

connections already below the viscosity maximum support this explanation, but of course cryo-TEM images do not allow a quantitative analysis of these structural changes. For these systems showing a viscosity decrease with ionic strength increase, we expect that the relaxation process after the viscosity maximum is described by a model based on the coupled reptation/reaction for branched micelles developed by Lequeux.²⁶ According to this model, the theoretical scaling exponent for the concentration dependence of the zero-shear viscosity is between ~ 2.4 and 3.2 . Experimental studies⁴⁷ show exponent values of 2.5 obtained at high salt content (1.5 M KBr) for the system CTAB/KBr² and 2.7 for the system CPyCl/NaSal at a NaSal concentration of 75 mM ($R = 0.75$).⁴⁸ These results confirm the assumption of relaxation of branched micelles. The formation of a saturated network of multiconnected micelles^{49,50} might be expected at the highest salt concentrations investigated here, and then a scaling exponent value less than 2 for the dependence of the viscosity on the surfactant concentration would be expected.^{2,49} A full study of the scaling exponent for the concentration dependence of the zero-shear viscosity in a broad range of salt concentrations would bring additional structural information. This will be addressed in a future article. For the CTAB/KBr system (Figure 4d) G_0 remains constant even in the high salt regime, but here the viscosity increases monotonically and does not go through a maximum.

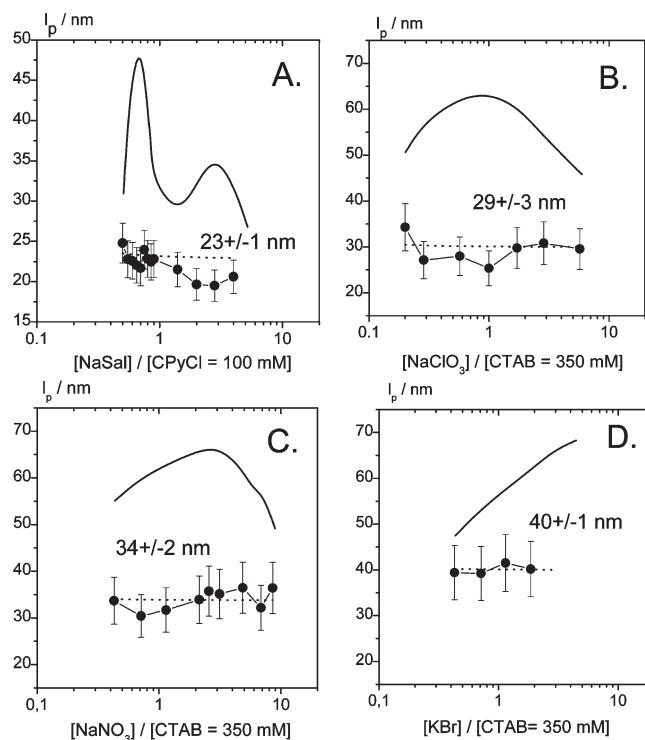


Figure 6. Variation of the persistence length l_p as a function of $R = [\text{salt}]/[\text{surfactant}]$ at constant surfactant concentration of 350 mM CTAB and 100 mM CPyCl obtained from DWS measurements: (A) CPyCl/NaSal (data redrawn from ref 14), (B) CTAB/NaClO₃, (C) CTAB/NaNO₃, and (D) CTAB/KBr and from OSF theory normalized to the DWS l_p value (dashed line). The solid line represents the variation of the zero-shear viscosity η_0 in arbitrary units.

The expected structure for this system is that of purely linear micelles.

4.2.3. Scission Energy of Wormlike Micelles. E_{sciss} is calculated from the temperature dependence of the ratio G''_{min}/G_0 according to eq 4. While the frequency range of oscillatory shear rheometry is not always sufficient to determine this minimum correctly, squeeze flow measurements yield reliable values and E_{sciss} is extracted from the slope of the semilogarithmic plot of G''_{min}/G_0 vs $1/T$ (cf. refs 14 and 51). The variation of E_{sciss} as a function of salt concentration is shown in Figure 5a–d for all systems. For the system with the penetrating salt (Figure 5a), E_{sciss} depends strongly and nonmonotonically on ionic strength, exhibiting two maxima corresponding to the variation of η_0 . Focusing only on the first viscosity maximum ($R = 0.65$), this increase corresponds to an increase of the average length of linear micelles due to the increased screening of the electrostatic repulsions between the charged headgroups. The decrease of E_{sciss} after the maximum is related to the formation of branching points.⁴⁶ In the latter case, the scission energy is related to the average contour length between branching points \bar{L}_C , and an increase in the number of branching points will lead to a decrease in \bar{L}_C , which corresponds to a decrease of E_{sciss} . For systems with nonpenetrating salt (Figure 5b–d), E_{sciss} is independent of ionic strength within experimental error. We expected an increase of the E_{sciss} with addition of salt, like for the system with penetrating counterion, but this variation is obviously very small and not detectable with our technique. This result confirms the hypothesis that

(47) Oelschlaeger, C.; Waton, G.; Candau, S. J. *Langmuir* **2003**, *19*, 10495–10500.

(48) Diploma Thesis Benedikt Lammerding, University of Karlsruhe, Germany, 2007.

(49) Appell, J.; Porte, G.; Khatory, A.; Kern, F.; Candau, S. J. *J. Phys. II* **1992**, *2*, 1045.

(50) Shikata, T.; Hirata, H.; Kotaka, T. *Langmuir* **1988**, *4*, 354–359.

(51) Couillet, I.; Hughes, T.; Maitland, G.; Candau, F.; Candau, S. J. *Langmuir* **2004**, *20*, 9541–9550.

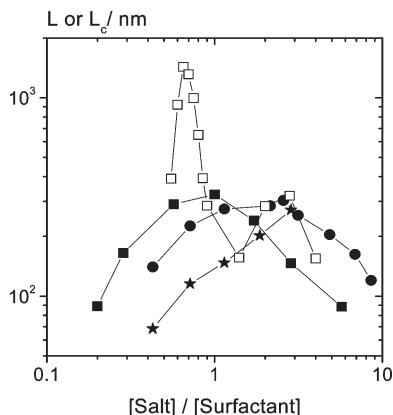


Figure 7. Dependence of the contour length \bar{L} or \bar{L}_C as a function of $R = [\text{salt}]/[\text{surfactant}]$ at constant surfactant concentration of 350 mM CTAB and 100 mM CPyCl obtained from oscillatory squeeze flow (squares). CPyCl/NaSal (open squares, data redrawn from ref 14), CTAB/NaClO₃ (solid squares), CTAB/NaNO₃ (solid circles), and CTAB/KBr (solid stars).

nonpenetrating counterions that bind only through polarizability effects do not strongly modify E_{sciss} , whereas penetrating counterions that enter the hydrophobic interior of the micelles modify this quantity clearly. A second observation is that E_{sciss} is independent of the nature of the added salt; the absolute value is almost similar for the three systems with $E_{\text{sciss}} \sim 17\text{--}20 k_B T$. This value is slightly higher compared to the CPyCl/NaSal system. Nevertheless, we expect a higher scission energy value for this latter system at the first viscosity maximum since both viscosity (Figure 3) and contour length (Figure 7) values are much higher compared to the systems with nonpenetrating counterions. Therefore, the scission energy data may indicate that for the CPyCl/NaSal system a significant amount of branched micelles exists already at the viscosity maximum, which is qualitatively confirmed by cryo-TEM images.⁴⁶ If the density of connections is sufficient, the scission energy value will be lower compared to the value for a system with only linear micelles.

4.2.4. Persistence Length of Wormlike Micelles. The persistence length l_p has been determined from the absolute value of G^* in the $\omega^{3/4}$ scaling regime according to eq 6. In order to obtain more reliable data in the ultrahigh-frequency regime (up to 10⁶ rad/s), we have applied a simple, self-consistent correction scheme to account for inertial effects when the motion of the tracer particles changes from Brownian to ballistic.¹⁴ For all systems investigated here the expected $\omega^{3/4}$ scaling is found for the inertia-corrected G'' data in a frequency range between 10⁵ and 10⁶ rad/s. We then fit the function $G'' = k_{\text{DWS}}\omega^{3/4}$ to the experimental data and calculate l_p from the resulting k_{DWS} value according to eq 6. This equation requires a lateral drag coefficient $\delta = 4\pi\eta_s \ln(0.6\lambda/d_{\text{mic}})$. The characteristic length λ is set equal to the mesh size, η_s is the solvent viscosity, and for the CTAB micelles diameter we insert $d_{\text{CTAB}} = 4.4 \text{ nm}$ ⁵² and $d_{\text{CPyCl}} = 2.6$ for CPyCl micelles.⁵³ This results in $\delta_{\text{CTAB}} = 0.008 \text{ N s/m}^2$ and $\delta_{\text{CPyCl}} = 0.005 \text{ N s/m}^2$. Figure 6a–d shows the variation of l_p with salt concentration from high-frequency DWS data. Our experimental results are systematically compared with the variation of l_p predicted by the Odijk–Skolnick–Fixman (OSF) theory.^{14,54,55} For the system with the penetrating salt (Figure 6a), l_p is independent of ionic strength within experimental error around the first viscosity

maximum. The average value of l_p is $23 \pm 1 \text{ nm}$. Then, l_p decreases from ~ 23 to $\sim 19 \text{ nm}$ when passing the second viscosity maximum. This decrease is significantly stronger than that predicted by OSF theory. We assume that the increase in flexibility is due to the incorporation of greater numbers of salicylate ions as R increases. Indeed, this effect can reverse the charge of the micelle from positive to negative, manifesting itself in changes of dynamical properties and can be responsible for the stronger increase in flexibility as compared to the electrostatic contribution. A similar behavior has been observed by Magid et al.⁵⁶ studying the mixed micellar system CTA26ClBz/CTACl upon addition of penetrating counterion 2,6-dichlorobenzoate. In that case increasing the amount of 2,6-dichlorobenzoate also lowers the bending modulus of the micelles; i.e., it makes them more flexible.

For systems with nonpenetrating salts (Figure 6b–d) l_p is independent of ionic strength within the experimental uncertainty throughout the experimental range and is consistent with the small l_p decrease ($< 1 \text{ nm}$) predicted by the OSF theory. But contrary to the scission energy, the persistence length significantly depends on the nature of the added salt. For CTAB/NaClO₃, CTAB/NaNO₃, and CTAB/KBr systems $l_p = 29 \pm 3$, 34 ± 2 , and $40 \pm 1 \text{ nm}$, respectively. The micellar flexibility increases with increasing the binding efficiency of the counterion. Moreover, the system with the penetrating salt is even more flexible than systems with nonpenetrating salts. A possible explanation resides in the relation between the micellar persistence length and the one-dimensional bending modulus, κ , of the micelle:

$$l_p = \frac{\kappa}{k_B T} \quad (10)$$

The persistence length or the corresponding bending modulus depends on the local environment of surfactant headgroups, hydrocarbon chains, and counterions. The bending modulus κ is considered to have two main contributions:⁵⁶ $\kappa = \kappa_{\text{ch}} + \kappa_{\text{hg}}$, with κ_{ch} being a steric contribution from changes in chain conformational free energy and κ_{hg} the contribution from the hydrocarbon/water interface and of headgroup/headgroup repulsion. For systems with nonpenetrating salts, only κ_{hg} is significant. This contribution is high when strong headgroup repulsion occurs, i.e., for system with low binding efficiency (KBr), and decreases for systems with stronger efficiency (NaClO₃); in the latter case the surface charge density is lowered, and thus the electrostatic contribution to the persistence length is reduced. Therefore, $l_p(\text{CTAB/NaClO}_3) < l_p(\text{CTAB/NaNO}_3) < l_p(\text{CTAB/KBr})$ is expected. The system with penetrating salt (CPyCl/NaSal) is even more flexible because an additional reduction of κ_{ch} . The impact of adding penetrating salt can be similar to the addition of short cosurfactants in mixed micellar systems. In the latter case the contribution of the surfactant chain to the overall modulus decreases as shown both experimentally and theoretically.^{56–59} In addition, increasing the aromatic counterion concentration decreases κ_{hg} as well, through its ability to decrease the micellar surface charge density and hence the short-range electrostatic resistance to bending. Thus, both contributions to the overall bending modulus are lower and responsible for the strong increase in flexibility for the system with penetrating counterion. Finally, using our l_p^{DWS} experimental values together with G_0 and G''_{min}

(56) Magid, L. J.; Han, Z.; Li, Z.; Butler, P. D. *J. Phys. Chem. B* **2000**, *104*, 6717–6727.

(57) May, S.; Ben-Shaul, A. *J. Chem. Phys.* **1995**, *103*, 3839–3848.

(58) Szleifer, I.; Kramer, D.; Ben-Shaul, A.; Gelbart, W. M.; Safran, S. A. *J. Chem. Phys.* **1990**, *92*, 6800–6817.

(59) Gradzielski, M.; Langevin, D.; Sottmann, T.; Strey, R. *J. Chem. Phys.* **1997**, *106*, 8232–8238.

(52) Nettekheim, F.; Wagner, N. *J. Langmuir* **2007**, *23*, 5267–5269.

(53) Fischer, P.; Rehage, H. *Rheol. Acta* **1997**, *36*, 13–27.

(54) Odijk, T. *Polym. Phys. Ed.* **1977**, *15*, 477–483.

(55) Skolnick, J.; Fixman, M. *Macromolecules* **1977**, *10*, 6717–6727.

from squeeze flow measurements, we calculated the contour length \bar{L} of the micelles from the equations $G''_{\min}/G_0 \approx l_c/\bar{L}$ with $l_c \approx \xi^{5/3}/l_p^{2/3}$ and $\xi = (k_B T/G_0)^{1/3}$. Figure 7 shows the dependence of \bar{L} as a function of R . For the CTAB/NaClO₃ and CTAB/NaNO₃ systems, \bar{L} exhibits one maximum analogous to the zero-shear viscosity and \bar{L}_{\max} is ~ 300 nm. This value is much lower compared to the CPyCl/NaSal system where \bar{L}_{\max} was $1.5 \mu\text{m}$. This result again confirms the hypothesis that nonpenetrating salts do not have an effect on the micellar growth or structure as strong as penetrating salts.

5. Conclusion

In this work we have used well-established experimental methods: high-frequency mechanical rheology and DWS to get new insight into structural and dynamic changes of aqueous wormlike micellar solutions formed from hexadecyltrimethylammonium bromide (CTAB) and different inorganic salts: potassium bromide (KBr), sodium nitrate (NaNO₃), and sodium chlorate (NaClO₃). We have investigated the dependence of G_0 , E_{sciss} , and l_p on concentration and binding efficiency of the salt systematically at constant surfactant concentration. Results for these systems with nonpenetrating counterions are compared to data for the system cetylpyridinium chloride (CPyCl) with the penetrating counterion sodium salicylate (NaSal). We found good agreement between mechanical rheology and DWS measurements in a broad frequency range. For the two systems CTAB/NaNO₃ and CTAB/NaClO₃, the zero-viscosity η_0 exhibits one maximum upon addition of salt, whereas for the CTAB/KBr system no maximum is observed. In contrast, the system CPyCl/NaSal exhibits two maxima. Obviously, the viscosity maximum shifts to higher R values, and the variation of viscosity with R is less pronounced as the binding efficiency decreases. The scission

energy, $E_{\text{sciss}} \sim 17\text{--}20 k_B T$, is independent of ionic strength and the binding strength of the salt within experimental errors for the three systems with nonpenetrating counterions and is slightly higher compared to the system CPyCl/NaSal, indicating that in the latter case a significant branching already occurs at the viscosity maximum. Concerning the salt effect on the persistence length, the weak variation of l_p is consistent with that predicted by the OSF theory, but l_p strongly depends on the nature of the salt. The micellar flexibility increases with the binding efficiency of the counterion according to the Hofmeister series. An even higher flexibility is found for the system with the penetrating salt which can be understood by a decrease of both the surfactant chain and headgroup contribution to the overall bending modulus. The plateau modulus G_0 varies upon addition of salt. At low salt concentration, G_0 increases strongly with increasing ion strength, which is attributed to an increase of the number of entanglements accompanying the growth of the micelles. In the region near the viscosity maximum, G_0 is independent of salt concentration for the three systems but increases slightly at very high salt content for the systems with NaClO₃ and NaNO₃. This slight increase is presumably due to the formation of branched micelles; at least for the CTAB/NaNO₃ system the existence of branching points has been proven independently by cryo-TEM images.⁴⁵ For the CTAB/KBr system, G_0 remains constant in the high salt regime. Unfortunately, up to now no cryo-TEM images exist for both CTAB/KBr and CTAB/NaClO₃ systems, further elucidating the structural changes due to the variation of the salt/surfactant ratio.

Acknowledgment. The authors thank F. Scheffold (Fribourg University, Switzerland) for fruitful discussions and his help with the inertia correction procedure. We acknowledge financial support from DFG Grant WI 3138/5-1.